Piezoelectric Electron-Phonon Interaction from *Ab Initio* Dynamical Quadrupoles: Impact on Charge Transport in Wurtzite GaN

Vatsal A. Jhalani,[1,*] Jin-Jian Zhou,[1,*] Jinsoo Park,[1] Cyrus E. Dreyer,[2,3] and Marco Bernardi[1,†]
[1]*Department of Applied Physics and Materials Science, California Institute of Technology, Pasadena, California 91125, USA*
[2]*Department of Physics and Astronomy, Stony Brook University, Stony Brook, New York 11794-3800, USA*
[3]*Center for Computational Quantum Physics, Flatiron Institute, 162 Fifth Avenue, New York, New York 10010, USA*

(Received 20 February 2020; accepted 27 August 2020; published 21 September 2020)

First-principles calculations of e-ph interactions are becoming a pillar of electronic structure theory. However, the current approach is incomplete. The piezoelectric (PE) e-ph interaction, a long-range scattering mechanism due to acoustic phonons in noncentrosymmetric polar materials, is not accurately described at present. Current calculations include short-range e-ph interactions (obtained by interpolation) and the dipolelike Frölich long-range coupling in polar materials, but lack important quadrupole effects for acoustic modes and PE materials. Here we derive and compute the long-range e-ph interaction due to dynamical quadrupoles, and apply this framework to investigate e-ph interactions and the carrier mobility in the PE material wurtzite GaN. We show that the quadrupole contribution is essential to obtain accurate e-ph matrix elements for acoustic modes and to compute PE scattering. Our work resolves the outstanding problem of correctly computing e-ph interactions for acoustic modes from first principles, and enables studies of e-ph coupling and charge transport in PE materials.

DOI: 10.1103/PhysRevLett.125.136602

When atoms move due to lattice vibrations, the potential seen by an electron quasiparticle changes due to both short-range and long-range forces. Early theories of such electron-phonon (e-ph) interactions focused on simplified models tailored to specific materials [1]. For example, the deformation potential, first formulated for metals, quantifies the e-ph interactions with acoustic phonons in the long-wavelength limit [2]. In ionic and polar covalent materials, in which atoms can be thought of as carrying a net charge, Fröhlich identified a dipolelike long-range e-ph interaction due to longitudinal optical (LO) phonons [3]. Also important is the piezoelectric (PE) e-ph interaction, which arises from the strain induced by acoustic phonons in polar materials lacking inversion symmetry [4,5]. Its conventional formulation by Mahan expresses the e-ph coupling in terms of the macroscopic PE constants of the material [5].

Vogl unified these e-ph interactions [6], showing that the dipole, PE, and deformation-potential contributions originate from a multipole expansion [7] of the e-ph potential, and analyzed its behavior in the long-wavelength limit (phonon wave vector $\mathbf{q} \to 0$). The Fröhlich dipole term diverges as $1/q$ in this limit, and it is proportional to the sum of atomic dipoles: if each atom κ is associated with a Born charge tensor, $\mathbf{Z}_\kappa$, contracting this tensor with the phonon eigenvector $\mathbf{e}_{\nu\mathbf{q}}$ gives the atomic contributions to the dipole field, $\mathbf{Z}_\kappa \mathbf{e}_{\nu\mathbf{q}}$. Next in the multipole expansion is the quadrupole field generated by the atomic motions, which approaches a constant value as $\mathbf{q} \to 0$. If each atom is associated with a dynamical quadrupole tensor, $\mathbf{Q}_\kappa$, the atomic quadrupole contributions can be written as $\mathbf{Q}_\kappa \mathbf{e}_{\nu\mathbf{q}}$. Both the dipole and the quadrupole terms contribute to the PE e-ph interaction [6]. The multipole expansion also gives octupole and higher terms, which vanish at $\mathbf{q} \to 0$ and can be grouped together into a short-range deformation potential.

Density functional theory (DFT) [8] and density functional perturbation theory (DFPT) [9] have enabled calculations of e-ph interactions from first principles. In turn, the e-ph interactions can be used in the Boltzmann transport equation (BTE) framework to predict electron scattering processes and charge transport [10–22]. The e-ph interactions computed with DFPT include all the contributions from the multipole expansion. Yet, DFPT is too costly to use directly on the ultrafine Brillouin zone grids needed to compute e-ph relaxation times and charge transport using the BTE. The current approach relies on Fourier interpolation techniques to capture the short-range e-ph interactions [23–26] while adding the dipole Fröhlich term in reciprocal space for polar materials. Deriving and computing the Fröhlich interaction [27,28] has been a first step toward implementing Vogl's modern e-ph theory in first-principles calculations and correctly capturing the long-range e-ph contributions. However, a key piece is still missing in the *ab initio* framework: the quadrupole e-ph interaction, which critically corrects the dipole term in polar materials, is sizable also in nonpolar materials, and is particularly important in PE materials such as wurtzite crystals or titanates.

In this Letter, we derive the *ab initio* quadrupole *e*-ph interaction and compute it for a PE material, wurtzite gallium nitride (GaN), using dynamical quadrupoles computed from first principles. We show that including the quadrupole term provides accurate *e*-ph matrix elements and is essential to obtaining the correct acoustic phonon contribution to carrier scattering. We compute the electron and hole mobilities in GaN including the quadrupole interaction, obtaining results in agreement with experiment. Our analysis highlights the large errors resulting from including only the Fröhlich term in GaN [29], which greatly overestimates the acoustic mode *e*-ph interactions [29,30]. Our companion paper [31] applies this framework to silicon and the PE material $PbTiO_3$. The quadrupole *e*-ph interaction, which critically corrects the dipole term in polar materials, is sizable in nonpolar materials, where it is the leading long-range *e*-ph interaction, and it is essential to correctly compute the *e*-ph matrix elements. Taken together, the quadrupole interaction completes the theory and enables accurate *ab initio* *e*-ph calculations in all materials and for all phonon modes.

The key ingredient in first-principles *e*-ph calculations are the *e*-ph matrix elements, $g_{mn\nu}(\mathbf{k},\mathbf{q})$, which encode the probability amplitude for scattering from an initial Bloch state $|n\mathbf{k}\rangle$ with band index n and crystal momentum $\mathbf{k}$ into a final state $|m\mathbf{k}+\mathbf{q}\rangle$ by emitting or absorbing a phonon with branch index ν and wave vector $\mathbf{q}$ [17,32]. Following Vogl [6], we separate the long-range dipole and quadrupole contributions from the short-range part:

$$g_{mn\nu}(\mathbf{k},\mathbf{q}) = g^{\text{dipole}}_{mn\nu}(\mathbf{k},\mathbf{q}) + g^{\text{quad}}_{mn\nu}(\mathbf{k},\mathbf{q}) + g^{\text{S}}_{mn\nu}(\mathbf{k},\mathbf{q}) \quad (1)$$

where g^{dipole} is the *ab initio* Fröhlich interaction written in terms of Born effective charges [27,28], g^{quad} is the quadrupole interaction written in terms of dynamical quadrupoles, and g^{S} collects octupole and higher-order short-range terms. For polar acoustic modes, $g^{\text{dipole}}+g^{\text{quad}}$ is a generalized replacement for the phenomenological PE *e*-ph coupling expressed in terms of the PE constants [4,5]. We derive the first-principles quadrupole *e*-ph interaction $g^{\text{quad}}_{mn\nu}(\mathbf{k},\mathbf{q})$ by superimposing two oppositely oriented dipole moments, as discussed in detail in our companion paper [31], and obtain:

$$g^{\text{quad}}_{mn\nu}(\mathbf{k},\mathbf{q}) = \frac{e^2}{\Omega\varepsilon_0}\sum_{\kappa}\left(\frac{\hbar}{2\omega_{\nu\mathbf{q}}M_\kappa}\right)^{1/2}\sum_{G\neq-\mathbf{q}}\frac{\frac{1}{2}(q_\alpha+G_\alpha)(Q^{\alpha\gamma}_{\kappa,\beta}\mathbf{e}^{(\kappa)}_{\nu\mathbf{q},\beta})(q_\gamma+G_\gamma)}{(q_\alpha+G_\alpha)\epsilon_{\alpha\gamma}(q_\gamma+G_\gamma)}\langle m\mathbf{k}+\mathbf{q}|e^{i(\mathbf{q}+\mathbf{G})\cdot(\mathbf{r}-\boldsymbol{\tau}_\kappa)}|n\mathbf{k}\rangle, \quad (2)$$

where e is the electron charge, Ω is the unit cell volume, M_κ and $\boldsymbol{\tau}_\kappa$ are the mass and position of the atom with index κ, $\mathbf{G}$ are reciprocal lattice vectors, $\mathbf{e}^{(\kappa)}_{\nu\mathbf{q}}$ is the phonon eigenvector projected on atom κ, and $\boldsymbol{\epsilon}$ is the dielectric tensor of the material. Summation over the Cartesian indices α, β, γ is implied.

The dynamical quadrupoles $\mathbf{Q}_\kappa$ entering Eq. (2) are third-rank tensors defined as the second order term in the long-wavelength expansion of the cell-integrated charge-density response to a monochromatic displacement [33–35]. Here, they are computed by symmetrizing the first-order-in-$\mathbf{q}$ polarization response [34,36]:

$$Q^{\alpha\gamma}_{\kappa,\beta} = i\Omega\left(\frac{\partial\bar{P}^{\mathbf{q}}_{\alpha,\kappa\beta}}{\partial q_\gamma}\bigg|_{\mathbf{q}=0} + \frac{\partial\bar{P}^{\mathbf{q}}_{\gamma,\kappa\beta}}{\partial q_\alpha}\bigg|_{\mathbf{q}=0}\right). \quad (3)$$

With the full first-principles *e*-ph matrix elements in Eq. (1) in hand, we compute the phonon-limited mobility at temperature T using the BTE in both the relaxation time approximation (RTA) and with a full iterative solution [17]. Briefly, we compute the *e*-ph scattering rates (and their inverse, the relaxation times $\tau_{n\mathbf{k}}$), from the lowest order *e*-ph self-energy [32]. The mobility is then obtained as the energy integral [17]:

$$\mu_{\alpha\beta}(T) = \frac{e}{n_c\Omega N_{\mathbf{k}}}\int dE\left(-\frac{\partial f}{\partial E}\right)\sum_{n\mathbf{k}}\boldsymbol{F}^{\alpha}_{n\mathbf{k}}(T)\mathbf{v}^{\beta}_{n\mathbf{k}}\delta(E-\varepsilon_{n\mathbf{k}}), \quad (4)$$

where n_c is the carrier concentration, f is the Fermi-Dirac distribution, $N_{\mathbf{k}}$ is the number of $\mathbf{k}$ points, and $\mathbf{v}_{n\mathbf{k}}$ and $\varepsilon_{n\mathbf{k}}$ are electron band velocities and energies, respectively. The $\boldsymbol{F}^{\alpha}_{n\mathbf{k}}$ term is obtained as $\tau_{n\mathbf{k}}(T)\mathbf{v}^{\alpha}_{n\mathbf{k}}$ in the RTA or by solving the BTE iteratively.

We carry out *ab initio* calculations on wurtzite GaN with relaxed lattice parameters, using the same settings as in our recent work [37]. The ground state properties and electronic wave functions are computed using DFT in the generalized gradient approximation [38] with the QUANTUM ESPRESSO code [39,40]. We include spin-orbit coupling by employing fully relativistic norm-conserving pseudopotentials [41,42] (generated with PSEUDO DOJO [43]) and correct the DFT band structure using *GW* results. We use DFPT [9] to compute phonon frequencies and eigenvectors, and obtain the *e*-ph matrix elements $g_{nm\nu}(\mathbf{k},\mathbf{q})$ on coarse $8\times8\times8$ $\mathbf{k}$-point and $\mathbf{q}$-point grids [44] using our PERTURBO code [17]. We obtain the dynamical quadrupoles $\mathbf{Q}_\kappa$ by computing $\bar{P}^{\mathbf{q}}_{\alpha,\kappa\beta}$ in Eq. (3) with the methodology in Ref. [36] as implemented in the ABINIT code [45].

All efforts were made to maintain consistency with the DFT and DFPT calculations and the results were validated against DFPT clamped-ion PE constants (see the Supplemental Material [46]). We subtract the long-range terms $g^{\text{dipole}} + g^{\text{quad}}$, interpolate the e-ph matrix elements using Wannier functions [48] to fine $\mathbf{k}$- and $\mathbf{q}$-point grids, and then add back the long-range terms. The resulting matrix elements are employed to compute relaxation times and mobilities [46] with the PERTURBO code [17].

Since DFPT can accurately capture the long-range e-ph interactions, it can be used as a benchmark for our approach of including the dipole plus quadrupole terms after interpolation. Note that due to computational cost, DFPT calculations cannot be carried out on the fine grids needed to compute electrical transport, so the long-range terms need to be added after interpolation. Following Ref. [27], we define a gauge-invariant e-ph coupling strength, D^{ν}_{tot}, proportional to the absolute value of the e-ph matrix elements:

$$D^{\nu}_{\text{tot}}(\mathbf{q}) = \hbar^{-1}\sqrt{2\omega_{\nu\mathbf{q}}M_{\text{uc}}\sum_{mn}|g_{mn\nu}(\mathbf{k}=\Gamma,\mathbf{q})|^2/N_b}, \quad (5)$$

with M_{uc} the unit cell mass and N_b the number of bands. We compute $D^{\nu}_{\text{tot}}(\mathbf{q})$ with various approximations to analyze the role of the quadrupole e-ph interactions.

In Fig. 1, we use $D^{\nu}_{\text{tot}}(\mathbf{q})$ obtained from direct DFPT calculations of the matrix elements as a benchmark, and compare calculations that include only the long-range Fröhlich dipole interaction and both the dipole and quadrupole interactions. The short-range e-ph interactions are included in both cases as a result of the Wannier interpolation. Including the quadrupole term dramatically improves the accuracy of the e-ph matrix elements for the longitudinal acoustic (LA) and transverse acoustic (TA) modes at small $\mathbf{q}$ (near Γ in Fig. 1). The discrepancy between the dipole-only calculation and DFPT is completely corrected when including the quadrupole term, which reproduces the DFPT benchmark exactly. While the dipole-only scheme leads to large errors, the dipole and quadrupole contributions, as can be seen, cancel each other out since they are nearly equal and opposite for acoustic modes in GaN. If the quadrupole correction is not included, in principle the interpolation could be improved at small $\mathbf{q}$ by using a denser $\mathbf{q}$-point grid when computing the DFPT matrix elements. However, due to the nonanalyticity of the quadrupole term, prohibitively dense DFPT grids are required to approach the accuracy of the quadrupole term [25].

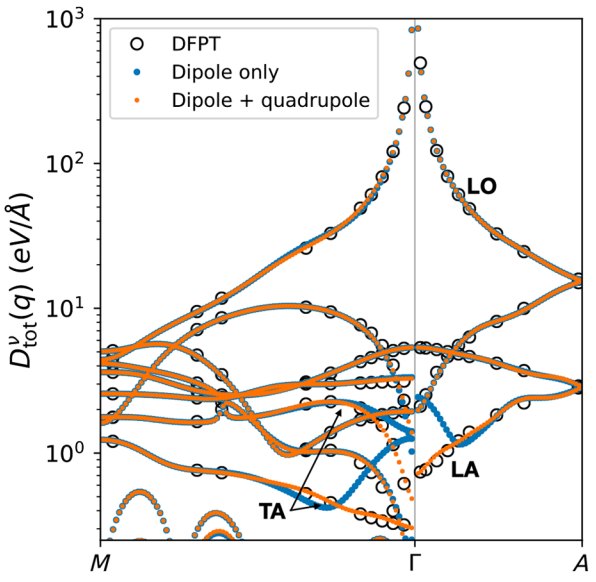

FIG. 1. Mode-resolved e-ph coupling strength, $D^{\nu}_{\text{tot}}(\mathbf{q})$, computed using the two lowest conduction bands; the initial state is fixed at Γ and $\mathbf{q}$ is varied along high-symmetry lines. The $D^{\nu}_{\text{tot}}(\mathbf{q})$ data computed with e-ph matrix elements from DFPT (black circles) is used as a benchmark, and compared with Wannier interpolation plus Fröhlich interaction (blue) or plus Fröhlich and quadrupole interactions (orange).

Both the dipole and quadrupole terms contribute to the PE e-ph interaction from the LA and TA acoustic modes [6]. Expanding the phonon eigenvectors at $\mathbf{q} \to 0$ as $\mathbf{e}_{\nu\mathbf{q}} \approx \mathbf{e}^{(0)}_{\nu\mathbf{q}} + iq\mathbf{e}^{(1)}_{\nu\mathbf{q}}$ [6], one finds two PE contributions of order q^0 for $\mathbf{q} \to 0$ [6]. One is from the Born charges, $\mathbf{Z}_{\kappa}(iq\mathbf{e}^{(1)}_{\nu\mathbf{q}})$, and is a dipolelike interaction generated by atoms with a net charge experiencing different displacements due to an acoustic mode. The other is from the dynamical quadrupoles, $\mathbf{Q}_{\kappa}\mathbf{e}^{(0)}_{\nu\mathbf{q}}$, and is associated with a clamped-ion electronic polarization [49]. As a result, the *ab initio* Fröhlich term includes only part of the PE e-ph interaction, so the dipole-only scheme fails in GaN because it neglects the all-important quadrupole electronic contribution. We also implemented and tested Mahan's phenomenological PE coupling [5],

$$\tilde{g}^{\text{PE}}_{\nu}(\mathbf{q}) = 4\pi\frac{e^2}{4\pi\varepsilon_0}\left[\frac{\hbar}{2\omega_{\nu\mathbf{q}}M_{\text{uc}}}\right]^{1/2}\frac{q_\alpha e_{\alpha,\beta\gamma}\mathbf{e}_{\nu\mathbf{q},\beta}q_\gamma}{q_\alpha\epsilon_{\alpha\gamma}q_\gamma}, \quad (6)$$

where $e_{\alpha,\beta\gamma}$ are the PE constants of GaN [46]. In the $\mathbf{q} \to 0$ limit, this model includes both ionic-motion and electronic effects [6], and is a less computationally demanding alternative that does not require computing the dynamical quadrupoles. We find that the e-ph coupling $D^{\nu}_{\text{tot}}(\mathbf{q})$ obtained from the Mahan model improves over the dipole-only scheme [46], but exhibits discrepancies with direct DFPT calculations at finite $\mathbf{q}$, and overall is inadequate for quantitative calculations.

Figure 2 shows the effect of using the more accurate quadrupole scheme on the e-ph scattering rates (defined as the inverse of the e-ph relaxation times, $\Gamma_{n\mathbf{k}} = 1/\tau_{n\mathbf{k}}$) computed at 300 K. We focus on the energy range of interest for charge transport near 300 K, namely an energy window within ∼100 meV of the band edges. Since these energies are below the LO phonon emission threshold

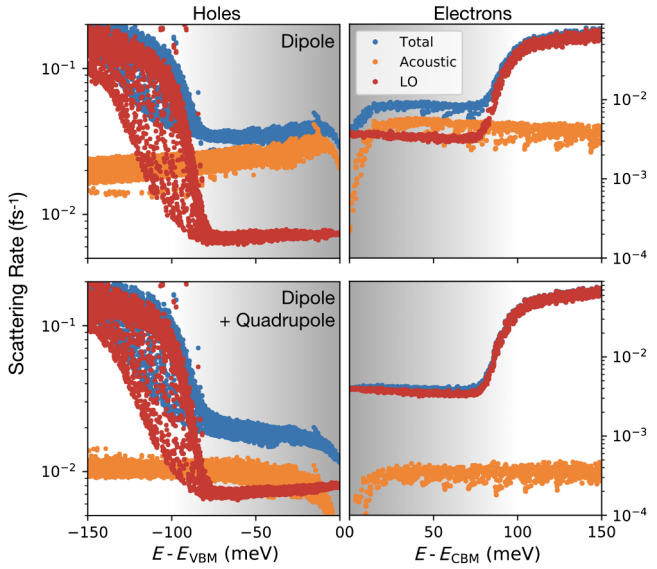

FIG. 2. Electron-phonon scattering rates at 300 K. We compare calculations including the long-range Fröhlich interaction only (top) with results including the Fröhlich and quadrupole interactions (bottom). The short-range e-ph interactions are included in both cases as a result of the interpolation. We plot the total scattering rate (blue) as well as the contributions from the LO (red) and acoustic (orange) modes for holes (left) and electrons (right) as a function of carrier energy within 150 meV of the band edges. The gray shading represents the energies at which carriers contribute to the mobility, as given by the integrand in Eq. (4). The hole and electron energy zeros are the valence and conduction band edges, respectively.

(90 meV in GaN), LO scattering is suppressed and dominated by thermally activated LO phonon absorption processes. On the other hand, there is a large phase space for acoustic phonon scattering, especially for interband processes in the valence band. For electrons, including the quadrupole term greatly suppresses the acoustic mode contribution to the scattering rates, reducing it from nearly half of the total scattering rate to a negligible contribution (Fig. 2). This result is due to the cancellation of the dipole and quadrupole terms for acoustic phonons discussed above. As expected, the LO contribution becomes dominant for electrons in the conduction band, where small-$\mathbf{q}$ intravalley scattering is controlled by the Fröhlich interaction with 1/q behavior rather than by the PE dipole and quadrupole terms, both of which have a q^0 trend at small $\mathbf{q}$. Using correct e-ph matrix elements that include the quadrupole term, our calculation restores this physical intuition.

A similar but less pronounced trend is found for holes in Fig. 2, where at the peak of the mobility integrand (~50 meV below the valence band edge) acoustic phonon scattering is suppressed from 75% of the total scattering rate when only the Fröhlich interaction is included to less than 50% when including the quadrupole term. The effect is less pronounced for holes due to the greater proportion of larger-$\mathbf{q}$ interband scattering channels in the valence band, which are less affected by the quadrupole interaction (see Fig. 1). Neglecting the quadrupole term in GaN may partially account for the large acoustic phonon scattering for holes found in recent calculations [29,30].

Analysis of the temperature dependent mobility in GaN, computed using Eq. (4) with both the RTA and iterative BTE approaches, highlights the key role of the quadrupole e-ph interaction. Figure 3 shows the electron and hole mobilities in the basal [1000] plane of GaN, computed both using Wannier interpolation plus the Fröhlich interaction and with our improved scheme including the quadrupole term. Experimental mobility measurements [50–56] are also given for comparison. Compared to calculations that include only the dipole Fröhlich interaction, including the quadrupole term removes the artificial overestimation of acoustic phonon scattering, thus increasing the computed mobility and correcting its temperature dependence, especially at lower temperatures, where acoustic scattering is dominant. For completeness, we also compare the electron mobility computed using e-ph matrix elements from Mahan's model [see Eq. (6)], and find that it underestimates the *ab initio* quadrupole result by up to 20% at 200 K and notably changes the temperature dependence of the mobility (see the Supplemental Material [46]). The error

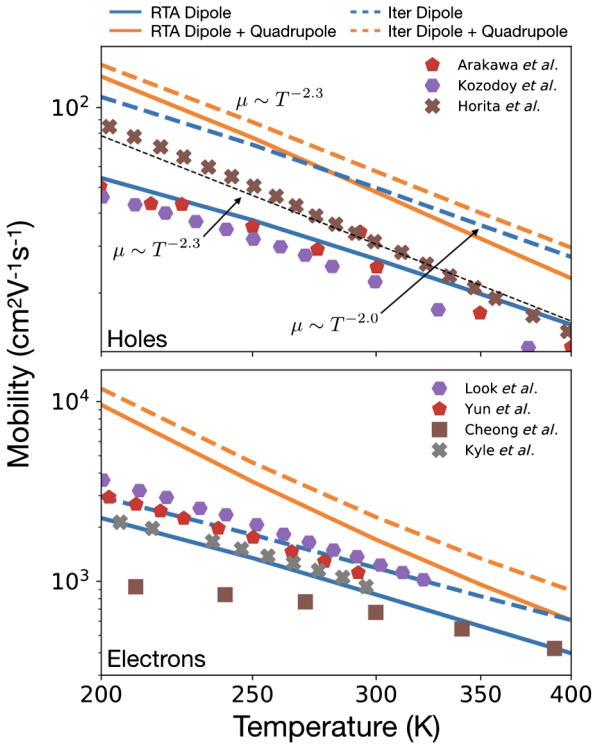

FIG. 3. Hole (top) and electron (bottom) mobilities in wurtzite GaN, computed in the [1000] plane. We show our computed results obtained with the RTA (solid lines) and iterative BTE (dashed lines), both with the long-range Fröhlich interaction only (blue) and with dipole plus quadrupole interactions (orange). Experimental results from Refs. [50–53] for electrons and Refs. [54–56] for holes are shown for comparison.

decreases at higher temperatures because the two methods differ primarily for small-$\mathbf{q}$ acoustic scattering, which becomes progressively less important at higher temperatures.

We find good agreement between our computed electron and hole mobilities and experimental results, especially when comparing with the highest mobilities measured in samples with low doping concentrations ($\sim 10^{15}$ cm^{-3} for n-type [50] and $\sim 10^{16}$–10^{17} cm^{-3} for p-type [54,57] GaN). In these high purity samples, charge transport is governed by phonon scattering in the temperature range we investigate, so these measurements are ideal for comparing with our phonon-limited mobilities.

We focus on the iterative BTE results, whose accuracy is superior to the RTA, also given for completeness [58]. For holes, in which acoustic scattering is significant, the temperature dependence of the mobility is improved after including the quadrupole interaction, as shown in the upper panel of Fig. 3. The exponent n in the temperature dependence of the mobility, $\mu \sim T^{-n}$, is $n = 2.3$ after including the quadrupole term, the same value as the exponent obtained by fitting the experimental data (for comparison, $n = 2.0$ in the dipole-only calculation). The temperature dependence of the electron mobility is only in reasonable agreement with experiment. Including two-phonon processes may be needed to further improve the temperature trend [59].

Our improved scheme increases the mobility values, placing them slightly above the experimental values. This trend is physically correct—our computed mobilities for an ideal crystal are an upper bound to the experimental mobilities. Other possible mechanisms not included in our calculations, such as the two-phonon scattering processes [59], are expected to lower the mobility and bring it in greater agreement with experiment.

In summary, we have presented a framework for computing the quadrupole e-ph interaction and including it in *ab initio* e-ph calculations. Our results show its crucial contribution to acoustic phonon and PE scattering. Our work enables accurate calculations of long-range acoustic phonon interactions and paves the way to studies of charge transport in PE materials.

V. J. thanks the Resnick Sustainability Institute at Caltech for fellowship support. J. P. acknowledges support by the Korea Foundation for Advanced Studies. This work was supported by the National Science Foundation under Grants No. DMR-1750613 for theory development and No. ACI-1642443 for code development. J.-J. Z. acknowledges partial support from the Joint Center for Artificial Photosynthesis, a DOE Energy Innovation Hub, as follows: the development of some computational methods employed in this work was supported through the Office of Science of the U.S. Department of Energy under Award No. DE-SC0004993. C. E. D. acknowledges support from the National Science Foundation under Grant No. DMR-1918455. The Flatiron Institute is a division of the Simons Foundation. This research used resources of the National Energy Research Scientific Computing Center, a DOE Office of Science User Facility supported by the Office of Science of the U.S. Department of Energy under Contract No. DE-AC02-05CH11231.

Note added.—Recently, we became aware of a related work by another group that reaches similar conclusions about the importance of the dynamical quadrupole term to obtain an accurate physical description of e-ph interactions [25,26].

*V. J. and J.-J. Z. contributed equally to this work.
†Corresponding author.
bmarco@caltech.edu

[1] J. M. Ziman, *Electrons and Phonons: The Theory of Transport Phenomena in Solids* (Oxford University Press, New York, 2001).
[2] J. Bardeen, Phys. Rev. **52**, 688 (1937).
[3] H. Fröhlich, Adv. Phys. **3**, 325 (1954).
[4] G. D. Mahan and J. J. Hopfield, Phys. Rev. Lett. **12**, 241 (1964).
[5] G. D. Mahan, *Condensed Matter in a Nutshell* (Princeton University Press, Princeton, 2011).
[6] P. Vogl, Phys. Rev. B **13**, 694 (1976).
[7] P. Lawaetz, Phys. Rev. **183**, 730 (1969).
[8] R. M. Martin, *Electronic Structure: Basic Theory and Practical Methods* (Cambridge University Press, Cambridge, England, 2004).
[9] S. Baroni, S. de Gironcoli, A. Dal Corso, and P. Giannozzi, Rev. Mod. Phys. **73**, 515 (2001).
[10] M. Bernardi, D. Vigil-Fowler, J. Lischner, J. B. Neaton, and S. G. Louie, Phys. Rev. Lett. **112**, 257402 (2014).
[11] J. I. Mustafa, M. Bernardi, J. B. Neaton, and S. G. Louie, Phys. Rev. B **94**, 155105 (2016).
[12] J.-J. Zhou and M. Bernardi, Phys. Rev. B **94**, 201201(R) (2016).
[13] V. A. Jhalani, J.-J. Zhou, and M. Bernardi, Nano Lett. **17**, 5012 (2017).
[14] N.-E. Lee, J.-J. Zhou, L. A. Agapito, and M. Bernardi, Phys. Rev. B **97**, 115203 (2018).
[15] J.-J. Zhou, O. Hellman, and M. Bernardi, Phys. Rev. Lett. **121**, 226603 (2018).
[16] J.-J. Zhou and M. Bernardi, Phys. Rev. Research **1**, 033138 (2019).
[17] J.-J. Zhou, J. Park, I.-T. Lu, I. Maliyov, X. Tong, and M. Bernardi, arXiv:2002.02045.
[18] W. Li, Phys. Rev. B **92**, 075405 (2015).
[19] T.-H. Liu, J. Zhou, B. Liao, D. J. Singh, and G. Chen, Phys. Rev. B **95**, 075206 (2017).
[20] J. Ma, A. S. Nissimagoudar, and W. Li, Phys. Rev. B **97**, 045201 (2018).
[21] T. Sohier, D. Campi, N. Marzari, and M. Gibertini, Phys. Rev. Mater. **2**, 114010 (2018).
[22] S. Poncé, W. Li, S. Reichardt, and F. Giustino, Rep. Prog. Phys. **83**, 036501 (2020).

[23] F. Giustino, M. L. Cohen, and S. G. Louie, Phys. Rev. B **76**, 165108 (2007).
[24] L. A. Agapito and M. Bernardi, Phys. Rev. B **97**, 235146 (2018).
[25] G. Brunin, H. P. C. Miranda, M. Giantomassi, M. Royo, M. Stengel, M. J. Verstraete, X. Gonze, G.-M. Rignanese, and G. Hautier, preceding Letter, Phys. Rev. Lett. **125**, 136601 (2020).
[26] G. Brunin, H. P. C. Miranda, M. Giantomassi, M. Royo, M. Stengel, M. J. Verstraete, X. Gonze, G.-M. Rignanese, and G. Hautier, companion paper, Phys. Rev. B **102**, 094308 (2020).
[27] J. Sjakste, N. Vast, M. Calandra, and F. Mauri, Phys. Rev. B **92**, 054307 (2015).
[28] C. Verdi and F. Giustino, Phys. Rev. Lett. **115**, 176401 (2015).
[29] S. Poncé, D. Jena, and F. Giustino, Phys. Rev. B **100**, 085204 (2019).
[30] S. Poncé, D. Jena, and F. Giustino, Phys. Rev. Lett. **123**, 096602 (2019).
[31] J. Park, J.-J. Zhou, V. A. Jhalani, C. E. Dreyer, and M. Bernardi, companion paper, Phys. Rev. B **102**, 125203 (2020).
[32] M. Bernardi, Eur. Phys. J. B **89**, 239 (2016).
[33] R. M. Martin, Phys. Rev. B **5**, 1607 (1972).
[34] M. Stengel, Phys. Rev. B **88**, 174106 (2013).
[35] M. Royo and M. Stengel, Phys. Rev. X **9**, 021050 (2019).
[36] C. E. Dreyer, M. Stengel, and D. Vanderbilt, Phys. Rev. B **98**, 075153 (2018).
[37] V. A. Jhalani, H.-Y. Chen, M. Palummo, and M. Bernardi, J. Phys. Condens. Matter **32**, 084001 (2019).
[38] J. P. Perdew, K. Burke, and M. Ernzerhof, Phys. Rev. Lett. **77**, 3865 (1996).
[39] P. Giannozzi *et al.*, J. Phys. Condens. Matter **21**, 395502 (2009).
[40] P. Giannozzi *et al.*, J. Phys. Condens. Matter **29**, 465901 (2017).
[41] D. R. Hamann, Phys. Rev. B **88**, 085117 (2013).
[42] J. P. Perdew, A. Ruzsinszky, G. I. Csonka, O. A. Vydrov, G. E. Scuseria, L. A. Constantin, X. Zhou, and K. Burke, Phys. Rev. Lett. **100**, 136406 (2008).
[43] M. van Setten, M. Giantomassi, E. Bousquet, M. Verstraete, D. Hamann, X. Gonze, and G.-M. Rignanese, Comput. Phys. Commun. **226**, 39 (2018).
[44] H. J. Monkhorst and J. D. Pack, Phys. Rev. B **13**, 5188 (1976).
[45] X. Gonze *et al.*, Comput. Phys. Commun. **205**, 106 (2016).
[46] See the Supplemental Material at http://link.aps.org/supplemental/10.1103/PhysRevLett.125.136602 for additional computational details, dynamical quadrupole calculations in wurtzite GaN, and phenomenological piezoelectric *e*-ph coupling results, which includes Ref. [47].
[47] D. R. Hamann, X. Wu, K. M. Rabe, and D. Vanderbilt, Phys. Rev. B **71**, 035117 (2005).
[48] A. A. Mostofi, J. R. Yates, G. Pizzi, Y.-S. Lee, I. Souza, D. Vanderbilt, and N. Marzari, Comput. Phys. Commun. **185**, 2309 (2014).
[49] F. Bernardini, V. Fiorentini, and D. Vanderbilt, Phys. Rev. B **56**, R10024 (1997).
[50] D. C. Look and J. R. Sizelove, Appl. Phys. Lett. **79**, 1133 (2001).
[51] F. Yun, M. Reshchikov, K. Jones, P. Visconti, H. Morkoç, S. Park, and K. Lee, Solid State Electron. **44**, 2225 (2000).
[52] M. G. Cheong, K. S. Kim, C. S. Oh, N. W. Namgung, G. M. Yang, C.-H. Hong, K. Y. Lim, E.-K. Suh, K. S. Nahm, H. J. Lee, D. H. Lim, and A. Yoshikawa, Appl, Phys. Lett. **77**, 2557 (2000).
[53] E. C. H. Kyle, S. W. Kaun, P. G. Burke, F. Wu, Y.-R. Wu, and J. S. Speck, J. Appl. Phys. **115**, 193702 (2014).
[54] Y. Arakawa, K. Ueno, A. Kobayashi, J. Ohta, and H. Fujioka, APL Mater. **4**, 086103 (2016).
[55] P. Kozodoy, H. Xing, S. P. DenBaars, U. K. Mishra, A. Saxler, R. Perrin, S. Elhamri, and W. C. Mitchel, J. Appl. Phys. **87**, 1832 (2000).
[56] M. Horita, S. Takashima, R. Tanaka, H. Matsuyama, K. Ueno, M. Edo, T. Takahashi, M. Shimizu, and J. Suda, Jpn. J. Appl. Phys. **56**, 031001 (2017).
[57] J. Suda and M. Horita, in *2016 Compound Semiconductor Week (CSW) [Includes 28th International Conference on Indium Phosphide Related Materials (IPRM) 43rd International Symposium on Compound Semiconductors (ISCS)]* (2016), pp. 1–2, https://doi.org/10.1109/ICIPRM.2016.7528835.
[58] For polar materials, the RTA mobility is typically lower than the more accurate mobility obtained with the iterative BTE, consistent with our results.
[59] N.-E. Lee, J.-J. Zhou, H.-Y. Chen, and M. Bernardi, Nat. Commun. **11**, 1607 (2020).